JCI insight

RESEARCH ARTICLE

# NOTCH3 regulates stem-to–mural cell differentiation in infantile hemangioma

**Andrew K. Edwards,[1] Kyle Glithero,[1,2] Peter Grzesik,[1,3] Alison A. Kitajewski,[1,4] Naikhoba C.O. Munabi,[1,5] Krista Hardy,[1,6] Qian Kun Tan,[1] Michael Schonning,[1] Thaned Kangsamaksin,[7] Jan K. Kitajewski,[8,9] Carrie J. Shawber,[1,8] and June K. Wu[1]**

[1]Department of Surgery, Columbia University College of Physicians and Surgeons, New York, New York, USA. [2]Department of Surgery, Maimonides Medical Center, Brooklyn, New York, USA. [3]Department of Anesthesia, University of Massachusetts Medical School, Worcester, Massachusetts, USA. [4]Department of Anatomy and Cell Biology, University of Illinois at Chicago, Chicago, Illinois, USA. [5]Department of Surgery, University of Southern California, Los Angeles, California, USA. [6]Department of Plastic Surgery, University of Texas Southwestern Medical Center, Dallas, Texas, USA. [7]Department of Biochemistry, Faculty of Science, Mahidol University, Bangkok, Thailand. [8]Department of Ob/Gyn, Columbia University College of Physicians and Surgeons, New York, New York, USA. [9]Department of Physiology and Biophysics, University of Illinois at Chicago, Chicago, Illinois, USA.

**Infantile hemangioma (IH) is a vascular tumor that begins with rapid vascular proliferation shortly after birth, followed by vascular involution in early childhood. We have found that NOTCH3, a critical regulator of mural cell differentiation and maturation, is expressed in hemangioma stem cells (HemSCs), suggesting that NOTCH3 may function in HemSC-to–mural cell differentiation and pathological vessel stabilization. Here, we demonstrate that NOTCH3 is expressed in NG2$^+$PDGFR$\beta^+$ perivascular HemSCs and CD31$^+$GLUT1$^+$ hemangioma endothelial cells (HemECs) in proliferating IHs and becomes mostly restricted to the $\alpha$SMA$^+$NG2$^{lo}$PDGFR$\beta^{lo}$ mural cells in involuting IHs. *NOTCH3* knockdown in HemSCs inhibited in vitro mural cell differentiation and perturbed $\alpha$SMA expression. In a mouse model of IH, *NOTCH3* knockdown or systemic expression of the NOTCH3 inhibitor, NOTCH3 Decoy, significantly decreased IH blood flow, vessel caliber, and $\alpha$SMA$^+$ perivascular cell coverage. Thus, NOTCH3 is necessary for HemSC-to–mural cell differentiation, and adequate perivascular cell coverage of IH vessels is required for IH vessel stability.**

## Introduction

Infantile hemangiomas (IHs) are benign vascular tumors with a distinct natural history and affect 4%–10% of the population (1, 2). A rapid proliferating phase occurs in the first 6–10 months of life, reaching a plateau phase at about 1 year. Involution begins at around 1 year of age and continues through childhood (1–3). In the early proliferative phase, IH tumors have poorly defined structures, but are highly cellular with glucose transporter 1–positive (GLUT1$^+$) cells, a hallmark of IH pathological vasculature (4). As IH progresses from proliferation towards its plateau phase, the endothelium becomes progressively organized and is surrounded by perivascular mural cells. During involution, IH vasculature gradually regresses over years. After IH involution is complete, a fibrofatty residuum with supernumerous capillary-sized blood vessels often remains. Although IHs are benign and eventually involute, the rapid growth during the proliferative phase can sometimes result in significant morbidity and mortality: bleeding, congestive heart failure, airway obstruction leading to respiratory distress, and permanent visual impairment (5, 6). Early intervention during the proliferative stage of IH can minimize the risk of development of potential complications. Recently, propranolol has shown efficacy. However, the mechanism of action is poorly understood (2), and rebound growth of IH can occur in up to 25% of patients when propranolol is tapered (7). Therefore, there is a need for alternative medical therapies.

IHs are proposed to arise from a hemangioma stem cell (HemSC) (3). HemSCs are CD133$^+$ and have a mesenchymal morphology and rapidly proliferate in vitro (8). HemSCs are pluripotent and form GLUT1$^+$ endothelial cells (ECs) in a xenograft mouse model of IH (3). Significant research has focused on the differentiation of HemSCs into hemangioma endothelial cells (HemECs) (8, 9). There is evidence that HemSCs can also differentiate into α smooth muscle actin$^+$ ($\alpha$SMA$^+$) mural cells in culture and in a xenograft mouse model

**Authorship note:** C.J. Shawber and J.K. Wu are co–senior authors.

**Conflict of interest:** TK, JKK, and CJS report that Columbia University and the authors have patents covering the work described herein: "Human NOTCH1 Decoys" (WO2013052607; TK, CJS, JK), "Composition of humanized NOTCH fusion proteins and methods of treatment" (US Patent 20110008342 A1; CJS, JK), and "Notch-based Fusion Proteins and Uses Thereof" (US Patent 7662919 B2; CJS, JK).

**Submitted:** March 9, 2017
**Accepted:** September 25, 2017
**Published:** November 2, 2017

**Reference information:**
*JCI Insight*. 2017;2(21):e93764.
https://doi.org/10.1172/jci.insight.93764.

(10), and we have shown that HemSCs are located in perivascular space and express mural cell markers such as αSMA, PDGFRβ, neuroglial proteoglycan 2 (NG2), and calponin (9, 10). However, the mechanisms and signaling pathways regulating HemSC differentiation into mural cells in IHs has yet to be elucidated.

Notch signaling is a conserved cell-to-cell communication regulatory pathway that modulates cell fate decisions in development. Four mammalian NOTCH proteins (NOTCH1–4) are activated by 4 ligands (Delta-like ligands: DLL1 and -4 and JAG1 and -2) that have been extensively studied because of their essential roles in developmental (11) and pathological angiogenesis (12, 13). We have previously published that NOTCH proteins are dynamically expressed and Notch signaling is activated in IH tissue and cells (9, 14). NOTCH3 is expressed in perivascular cells in IH tissues, and HemSCs in vitro. In the adult vasculature, NOTCH3 expression is mostly restricted to perivascular mural cells, pericytes, and vascular smooth muscle cells (VSMCs) (15, 16). Mutations in NOTCH3 are associated with CADASIL (cerebral autosomal dominant arteriopathy with subcortical infarcts and leukoencephalopathy), a hereditary cerebrovascular disease characterized by progressive VSMC death leading to hemorrhage and ministrokes in midlife (17, 18). *Notch3*-null mice are embryonically viable, but their VSMCs fail to properly differentiate and die via apoptosis beginning at 3 months of age (19). *Notch3* deletion in a *Notch1* heterozygous background led to arteriovenous malformations in the murine retina (16). Mural cell NOTCH3 has been proposed to be activated by endothelial JAG1, leading to increased NOTCH3 expression, as well as upregulation of the mural cell proteins αSMA and PDGFRβ (20). Thus, NOTCH3 may function to regulate HemSC differentiation into perivascular mural cells in IH. Consistent with this model, knockdown of endothelial JAG1 disrupted IH development in a xenograft model that was associated with an absence of mural cell coverage (10).

In the present study, we demonstrate that NOTCH3 is essential for HemSC differentiation into mural cells in IH. Disruption of NOTCH3 function via knockdown or expression of a NOTCH3 inhibitor, NOTCH3 Decoy (N3 Decoy), disrupted IH development in a xenograft IH mouse model. Our study supports the use of therapeutics that target NOTCH3 for medical management of IH.

## Results

*NOTCH3 expression in HemECs and perivascular cells in proliferating IHs becomes enriched in mural cells in involuting IHs*. Prior to determining NOTCH3 expression, we defined the expression of EC and perivascular cell proteins in proliferating and involuting IHs. Early proliferative IHs consist of dense clusters of cells in poorly organized vasculature structures with rounded lumenal ECs surrounded by perivascular cells, and stromal cells in the periphery (Supplemental Figure 1; supplemental material available online with this article; https://doi.org/10.1172/jci.insight.93764DS1). The lumenal cells expressed both CD31 and the IH-specific GLUT1, consistent with them being HemECs, whereas the surrounding perivascular cells were negative for both proteins (Figure 1A). In proliferating IHs, low levels of αSMA expression were observed in both the lumenal and perivascular cells (Figure 1B). As IHs continue from the proliferative phase to the involuting phase, IH tissues have decreased cellular density, and the lumenal cells take on an endothelial morphology surrounded by multiple layers of elongated perivascular mural cells (Supplemental Figure 1). In involuting IHs, $CD31^+GLUT1^+$ HemECs line the vessel lumens (Figure 1A and Supplemental Figure 2A) surrounded by $CD31^-GLUT1^-\alpha SMA^+$ perivascular cells (Figure 1B and Supplemental Figure 2B). The morphology, circumferential orientation, and αSMA expression of the perivascular cells are consistent with a VSMC phenotype.

In proliferating IHs, NOTCH3 was expressed in the $CD31^+$ HemECs and the surrounding $\alpha SMA^-$ and $\alpha SMA^+$ perivascular cells, with the highest expression observed in the $CD31^-\alpha SMA^-$ perivascular cells (Figure 1, C and D, and Supplemental Figure 2, C and D). A low level of NOTCH3 expression was also seen in the stromal cells. In involuting IHs, NOTCH3 expression becomes mostly restricted to the $\alpha SMA^+$ mural cells (Figure 1, C and D, and Supplemental Figure 2, C and D). Occasional $NOTCH3^+CD31^+$ ECs were also observed (Figure 1C), suggesting that NOTCH3 expression persists in a subset of HemECs during involution. We next costained for GLUT1 and NOTCH3 to determine if NOTCH3 was expressed in the $GLUT1^+$ HemECs. NOTCH3 was coexpressed in a subset of $GLUT1^+$ cells in proliferating IHs and $GLUT1^+$ lumenal cells in involuting IHs (Supplemental Figure 3). In summary, NOTCH3 was differentially expressed in multiple cell types (stromal, perivascular, and lumenal) in proliferative IHs, and its expression becomes restricted to the mural cells and a small subset of HemECs in involuting IHs.

*Dynamic and altered expression of perivascular cell proteins in proliferating and involuting IHs*. To characterize the perivascular cells, proliferating and involuting IH tissues were stained for the pan vascular mural cell

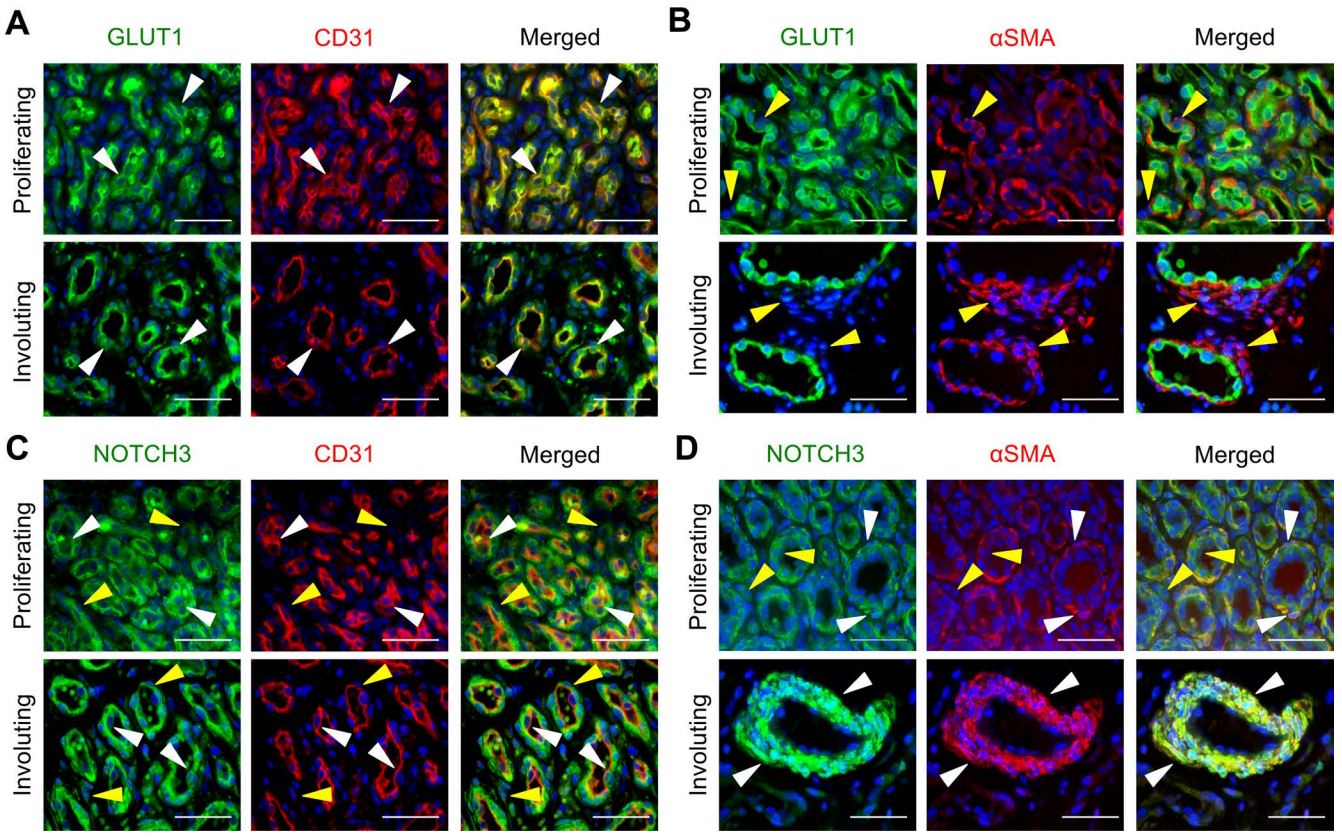


**Figure 1. NOTCH3 is expressed in perivascular and lumenal cells in IHs.** Serial sections of proliferating and involuting infantile hemangioma (IH) specimens were stained. (**A**) GLUT1 and CD31 costaining. White arrowheads mark GLUT1$^+$CD31$^+$ cells. Proliferating IH $n$ = 2, involuting IH $n$ = 3. (**B**) GLUT1 and αSMA costaining. Yellow arrowheads mark αSMA$^+$GLUT1$^-$ perivascular cells. Proliferating IH $n$ = 2, involuting IH $n$ = 7. (**C**) NOTCH3 and CD31 costaining. White arrowheads mark NOTCH3$^+$CD31$^+$ cells. Yellow arrowheads mark NOTCH3$^+$CD31$^-$ cells. Proliferating IH $n$ = 4, involuting IH $n$ = 5. (**D**) NOTCH3 and αSMA costaining. White arrowheads mark NOTCH3$^+$αSMA$^+$ perivascular cells. Yellow arrowheads mark NOTCH3$^+$αSMA$^-$ lumenal cells. Proliferating IH $n$ = 5, involuting IH $n$ = 8. Scale bars: 50 μm. The total number of IH specimens assessed for each antigen is presented in Supplemental Table 3. αSMA, α smooth muscle actin; GLUT1, glucose transporter 1.

marker PDGFRβ, the pericyte marker NG2, and the VSMC marker αSMA. In proliferating IHs, PDGFRβ was expressed in the majority of cells, with highest expression in the αSMA$^+$CD31$^-$ perivascular cells (Figure 2, A and B, and Supplemental Figure 4, A and B). In contrast, NG2 expression was observed in a subset of αSMA$^+$ perivascular cells and CD31$^+$ lumenal cells, where CD31 expression was apically expressed (Figure 2, C and D, and Supplemental Figure 4, C and D). NG2$^+$αSMA$^-$ cells were also seen interspersed in the stroma (Figure 2, C and D, and Supplemental Figure 4, C and D).

In involuting IH specimens, PDGFRβ expression was strongest in the CD31$^+$ HemECs, while its expression in αSMA$^+$ perivascular cells was reduced when compared with proliferating IHs (Figure 2, A and B). Similarly, NG2 was weakly expressed in the αSMA$^+$ mural cells and strongly expressed in CD31$^+$ HemECs during involution (Figure 2, C and D). In addition, PDGFRβ$^+$αSMA$^-$ and NG2$^+$αSMA$^-$ cells were seen interspersed in the stroma where residual HemSCs reside.

To further characterize the expression of perivascular and endothelial markers in HemSCs, expression of PDGFRβ, NG2, αSMA, CD31, GLUT1, and NOTCH3 in CD133$^+$ HemSCs was determined by immunofluorescence, FACS, and quantitative reverse transcription PCR (qRT-PCR). Consistent with the immunostaining of the perivascular cells in proliferating IH tissues, HemSCs expressed PDGFRβ, NG2, and NOTCH3 (Supplemental Figure 5). A small subset of HemSCs expressed the endothelial markers GLUT1 and CD31 (Supplemental Figure 5, A and B). Thus, HemSCs express multiple mural cell markers with inconsistent or absent expression of IH endothelial markers.

Taken together, the data demonstrate that perivascular cell proteins are dynamically and abnormally expressed in IH pathogenesis (Supplemental Table 1). PDGFRβ$^+$αSMA$^+$ and NG2$^+$αSMA$^+$ perivascular

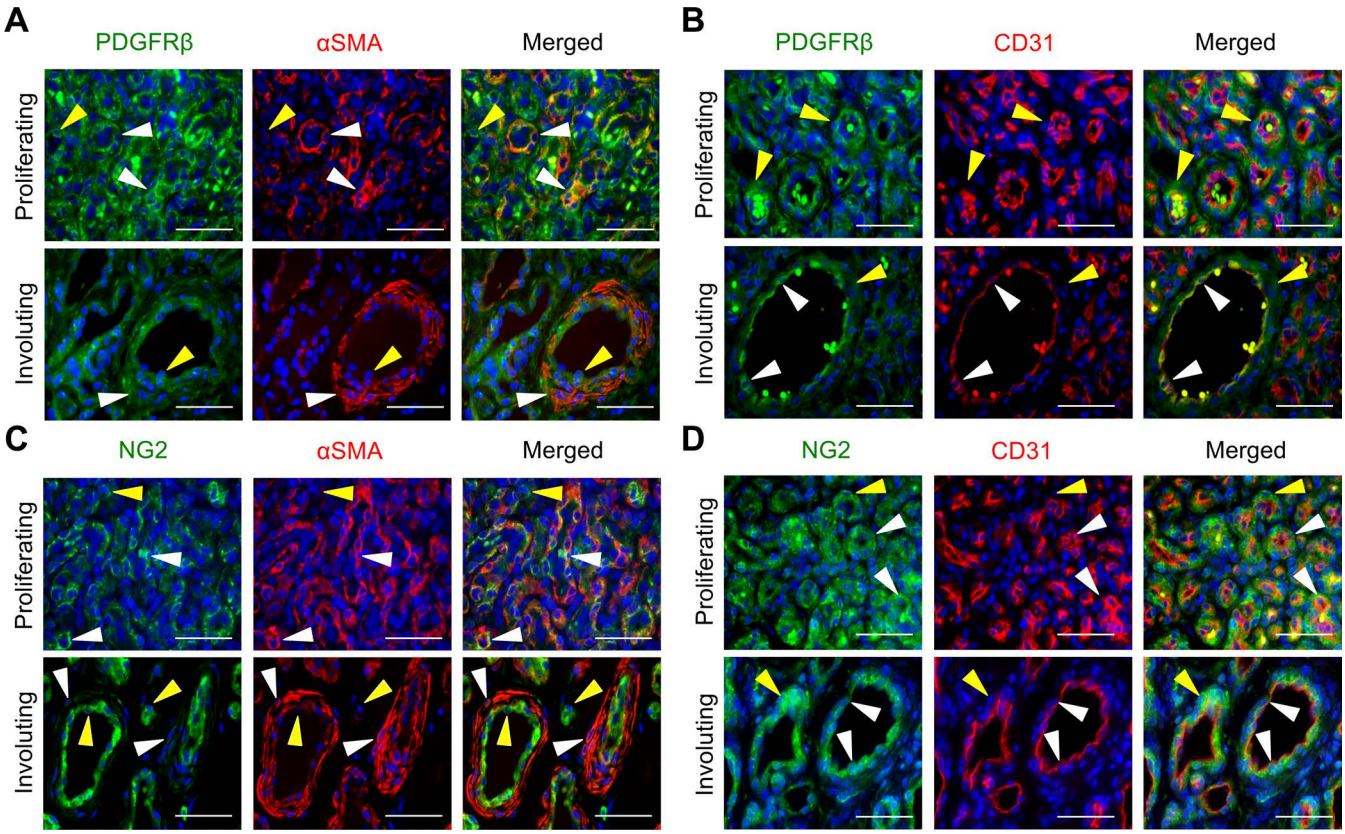


**Figure 2. Perivascular PDGFRβ and NG2 expression is decreased and misexpressed in lumenal endothelial cells during IHs progression.** Serial sections of proliferating and involuting infantile hemangioma (IH) specimens were stained. (**A**) PDGFRβ and αSMA costaining. White arrowheads mark PDGFRβ$^+$αSMA$^+$ perivascular cells. Yellow arrowheads mark PDGFRβ$^+$αSMA$^-$ lumenal cells. Proliferating IH $n$ = 2, involuting IH $n$ = 3. (**B**) PDGFRβ and CD31 costaining. White arrowheads mark PDGFRβ$^+$CD31$^+$ lumenal endothelial cells. Yellow arrowheads mark PDGFRβ$^+$CD31$^-$ perivascular cells. Proliferating IH $n$ = 3, involuting IH $n$ = 2. (**C**) NG2 and αSMA costaining. White arrowheads mark NG2$^+$αSMA$^+$ cells, and yellow arrowheads mark NG2$^+$αSMA$^-$ cells. Proliferating IH $n$ = 7, involuting IH $n$ = 7. (**D**) NG2 and CD31 costaining. White arrowheads mark NG2$^+$CD31$^+$ cells, and yellow arrowheads mark NG2$^+$CD31$^-$ cells. Proliferating IH $n$ = 7, involuting IH $n$ = 3. Scale bars: 50 μm. The total number of IH specimens assessed for each antigen is presented in Supplemental Table 3. αSMA, α smooth muscle actin; NG2, neuron-glial antigen 2.

cells were present in proliferating IHs, but both NG2 and PDGFRβ expression in mural cells was reduced, with NG2 only weakly expressed in perivascular cells during involution (Figure 2, A and B). In proliferating IHs, HemECs did not express PDGFRβ (Figure 2C), but expressed NG2 (Figure 2D). By contrast, HemECs in involuting IHs expressed PDGFRβ and demonstrated increased expression of NG2 (Figure 2, C and D), which was not expected as ECs do not normally express PDGFRβ and NG2 (21, 22).

*NOTCH3 is necessary for HemSCs to differentiate into αSMA$^+$ mural cells in vitro*. We assessed the role of NOTCH3 in HemSC-to–mural cell differentiation in 2 assays: (a) TBF-β–induced differentiation and (b) a HemSCs and endothelial colony-forming cells (ECFCs) coculture system. Initially, we evaluated the expression of the mural cell proteins, αSMA and PDGFRβ, in these systems. In culture, HemSCs expressed PDGFRβ and did not express αSMA (Supplemental Figure 5, A and C). When cultured in TBF-β–containing mural cell differentiation media for 2 weeks, HemSCs upregulated the expression αSMA (Figure 3A). In contrast, HemSCs maintained in growth medium expressed minimal αSMA.

The induction of αSMA in HemSCs was also observed in the HemSC/ECFC coculture assay. In this assay, HemSC-ECFC cell contact induces mural cell differentiation (10). When GFP$^+$ HemSCs were cocultured with ECFCs for 9 days, there was an increase in αSMA expression (Figure 3, B–D). Similar to tissue staining of proliferating involuting IHs, a decrease in PDGFRβ expression was observed (Figure 3, B–D). Thus, differentiation of pluripotent HemSCs into mural cells in vitro was consistent with the in vivo findings that demonstrated weaker PDGFRβ expression in αSMA$^+$ mural cells (Figure 2, A and C, and Supplemental Figure 4).

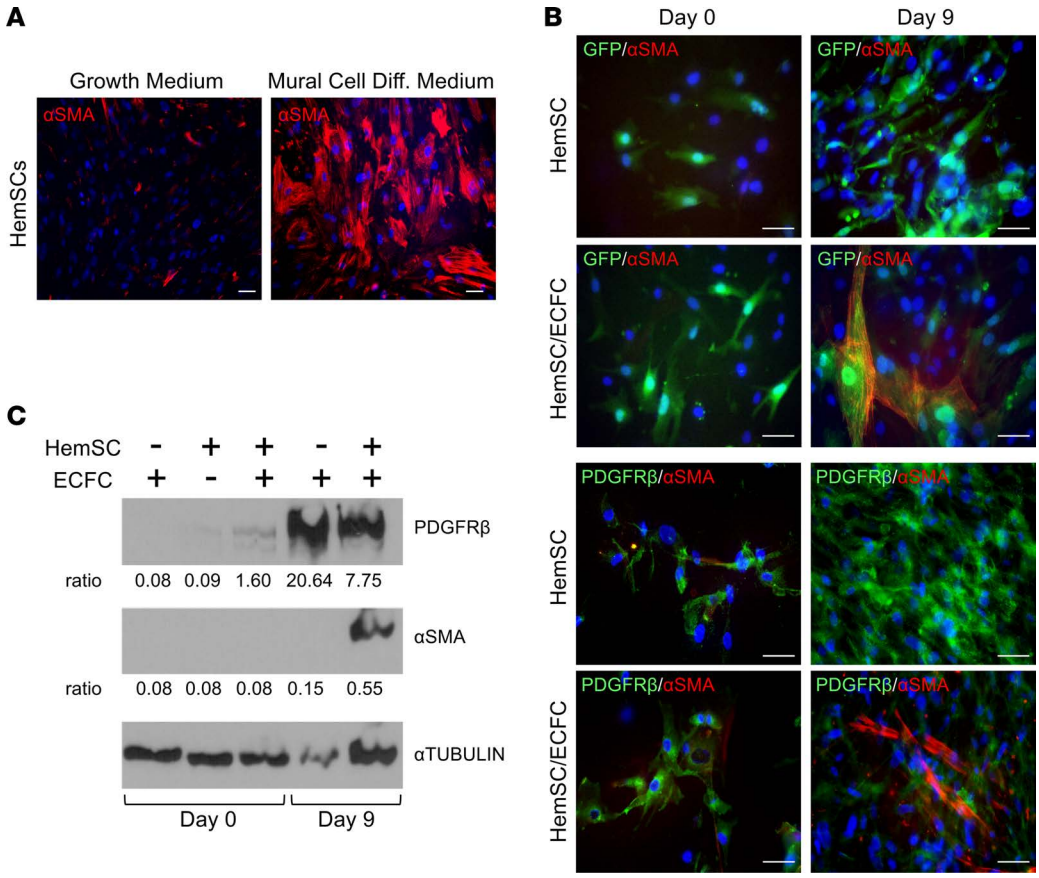


**Figure 3. HemSCs differentiate into αSMA$^+$PDGFRβ$^{lo}$ mural cells in culture.** (**A**) HemSCs ($n$ = 3) were grown either in growth or mural cell differentiation media for 2 weeks and stained for αSMA. (**B**) GFP$^+$ HemSCs ($n$ = 3) alone or cocultured with ECFCs in growth media were stained for αSMA or PDGFRβ at day 0 and 9. (**C**) Day 0 and 9 lysates from HemSC and HemSC/ECFC cocultures ($n$ = 3) were subjected to Western analysis, and probed with antibodies against PDGFRβ, αSMA, or α-TUBULIN as a loading control. Representative data from 3 independent HemSC populations done a total of 10 times are presented. The ratio of PDGFRβ and αSMA band intensity normalized by α-TUBULIN band intensity is presented below each image. Scale bars: 50 μm. αSMA, α smooth muscle actin; ECFC, endothelial colony-forming cell; Diff, differentiation, HemSC, hemangioma stem cell.

To determine the role of NOTCH3 in HemSC differentiation into mural cells, we generated HemSCs with *NOTCH3* knockdown (N3KD) by using a *NOTCH3* shRNA that were compared to HemSCs engineered to express scrambled (Scr) shRNA. Reduced *NOTCH3* expression correlated with a specific transcriptional downregulation of the Notch effectors, *HES1* and *HEYL* (Figure 4, A–C). *NOTCH1* and the Notch effectors, *HEY1* and *HEY2*, which are also expressed by HemSCs (9), were not significantly changed (Supplemental Figure 6A). Pericytes isolated from IH specimens have been suggested to promote angiogenesis (10). Therefore, we determined if N3KD altered the expression of the proangiogenic factors, *VEGFA*, *ANG1* (angiopoietin 1), and *ANG2* (angiopoietin 2). Their transcript levels were significantly decreased in N3KD HemSCs relative to Scr HemSCs (Supplemental Figure 6B). However, Notch3 inhibition did not consistently alter HemSC proliferation (data not shown), suggesting the HemSCs are not responding to changes in these angiogenic stimuli. N3KD in HemSCs specifically downregulated the expression of the Notch effectors, *HES1* and *HEYL*, and angiogenic factor expression, while it did not affect the expression of *HEY1* or *HEY2*, or cell proliferation.

We used the N3KD HemSCs and the Scr HemSCs in TGF-β–induced mural cell differentiation and HemSC/ECFC coculture assays. In the monoculture assay, TGF-β–induced αSMA expression was blocked in N3KD HemSCs (Supplemental Figure 7). When compared with control Scr HemSCs, αSMA expression was lower in the N3KD HemSCs in the HemSC/ECFC coculture assay at all time points (Figure 4, D and E). N3KD HemSCs had the highest αSMA expression at day 7 before decreasing at day 9 (Figure 4E). Together, these data demonstrate that NOTCH3 signaling is necessary for HemSC-to–mural cell differentiation in vitro.

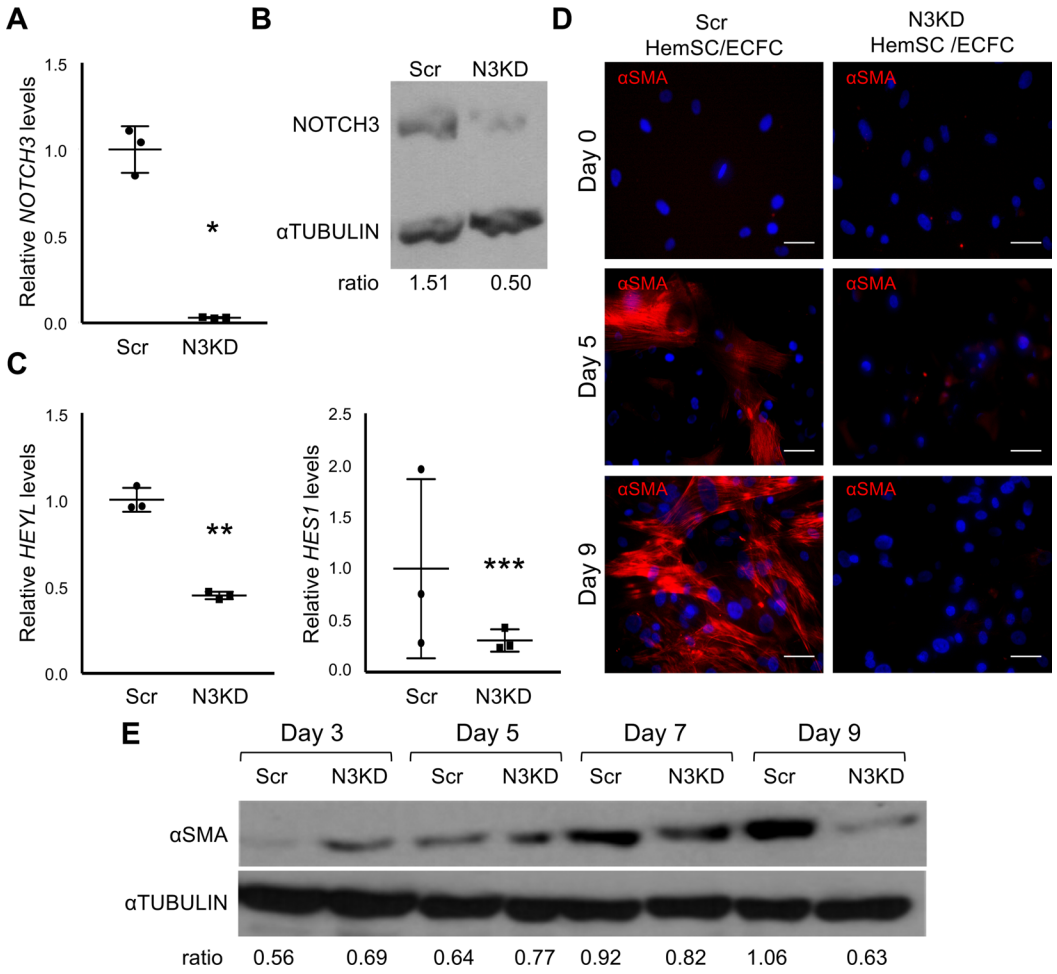


**Figure 4. NOTCH3 is necessary for HemSC mural cell differentiation.** (**A**–**C**) Assessment of *NOTCH3* knockdown (N3KD) in HemSCs. (**A**) Relative *NOTCH3* transcript levels in control HemSCs (Scr), and N3KD HemSCs determined by qRT-PCR and normalized by *BACTIN*. Representative data from 4 independent N3KD HemSC populations and matching Scr HemSC populations are presented. Error bars represent ± SD. $^{*}P < 0.007$, Student's *t* test. (**B**) Representative data of Western analysis from 2 independent N3KD and matching Scr HemSC lysates probed with antibodies against NOTCH3 or α-TUBULIN as a loading control. (**C**) Relative *HEYL* and *HES1* transcript levels in Scr and N3KD HemSCs determined by qRT-PCR and normalized by *BACTIN* expression. Representative data presented from 3 independent HemSC populations done in duplicate. Error bars represent ± SD. $^{**}P < 0.0007$, $^{***}P < 0.05$, Student's *t* test. (**D**) Scr HemSCs ($n = 3$) or N3KD HemSCs ($n = 3$) cocultured with ECFCs in growth media were stained for αSMA at days 0, 5, and 9. Scale bars: 50 μm. (**E**) Day 3, 5, 7, and 9 lysates from Scr and N3KD HemSC/ECFC cocultures were subjected to Western analysis, and probed with antibodies against αSMA or α-TUBULIN as a loading control. Ratio of αSMA band intensity normalized by α-TUBULIN band intensity presented below. Representative data from 3 Scr and N3KD HemSC populations and experiments perform in duplicate for each HemSC population. αSMA, α smooth muscle actin; ECFC, endothelial colony-forming cell; HemSC, hemangioma stem cell; Scr, scrambled.

*Inhibition of NOTCH3 activity in HemSCs suppresses IH vessel formation in vivo*. In order to test the role of NOTCH3 in mural cell differentiation in IH pathobiology, we used a coculture IH mouse model. In this model, HemSCs are resuspended in Matrigel in a 1:1 ratio with ECFCs and injected subcutaneously in the flanks of immunocompromised mice. As compared with implants with HemSCs alone, HemSC/ECFC implants form a robust IH-like phenotype (Supplemental Figure 8) with Dopplerable blood flow as early as 1 week after implantation (data not shown). Three different N3KD HemSC populations and matching controls were assessed in this IH mouse model. As compared with Scr HemSC/ECFC implants, N3KD HemSC/ECFC implants had significantly reduced Doppler-detectable blood flow (Figure 5, A and B). Although vessel density did not differ, there was a significant decrease in vessel caliber in the N3KD HemSC/ECFC implants as compared with Scr HemSC/ECFC implants (Figure 5, C and D). The decrease in vessel caliber correlated with reduced $\alpha SMA^{+}$ mural cell density, as well as a significant reduction in αSMA expression in mural cells that were present in the N3KD HemSC/ECFC implants (Figure 5, E and F). Thus, loss of *NOTCH3* in HemSCs resulted in decreased mural cell coverage, and

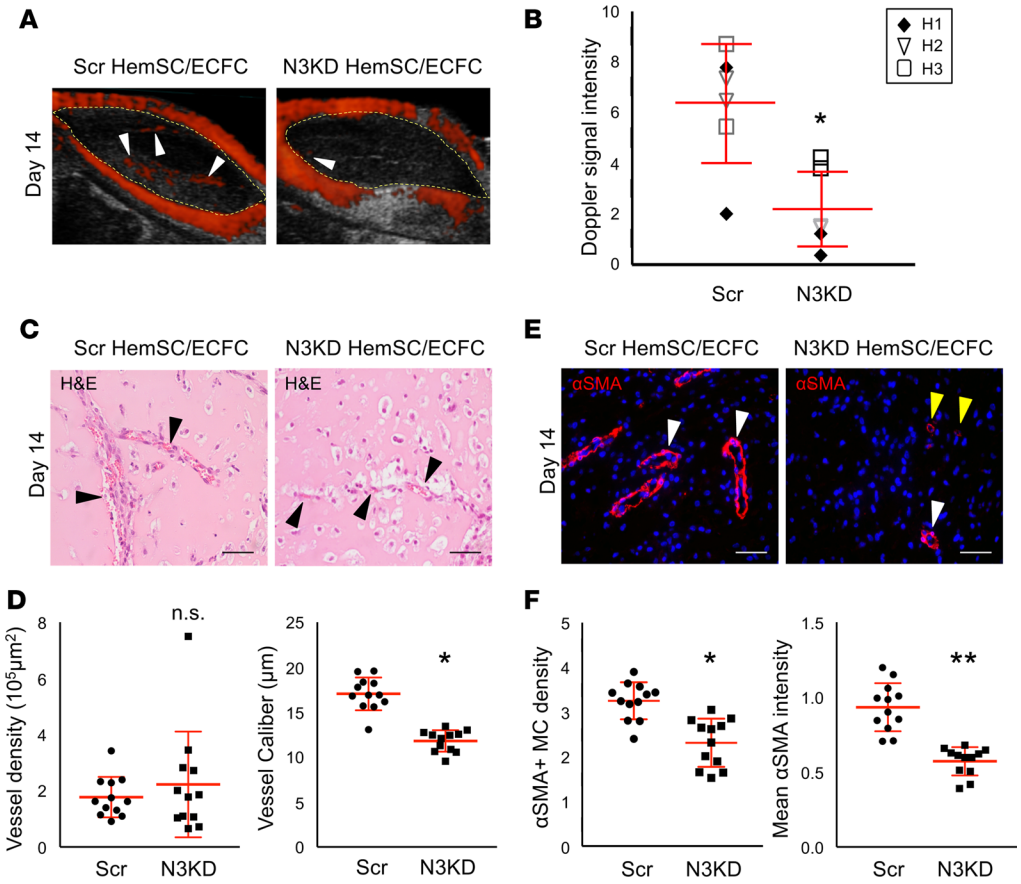


**Figure 5. NOTCH3 activity is required for HemSC mural cell differentiation and IH development in a mouse model of IH.** *NOTCH3*-knockdown (N3KD) HemSCs or Scr HemSCs in a 1:1 ratio with ECFCs were resuspended in Matrigel, and subcutaneously implanted into the flanks of immunocompromised mice. (**A**) Detection of high blood flow by ultrasound Doppler in Scr HemSC/ECFC and N3KD HemSC/ECFC xenografts at day 14 after implantation. Xenograft area marked with yellow dotted line. White arrowheads mark Dopplerable blood flow (red). (**B**) Scatter plot of mean Doppler signal intensity normalized by xenograft area ($n$ = 3 populations: H1, H2, H3; $n$ = 2 implants each). Average mean intensity denoted with a horizontal line. Error bars represent ± SD. *$P$ < 0.03, 1-way ANOVA. (**C**) H&E staining of Scr HemSC/ECFC and N3KD HemSC/ECFC xenograft sections. Arrowheads mark red blood cell–containing vessels. (**D**) Quantification of vessel density and caliber ($n$ = 3 populations; $n$ = 2 implants each). Error bars represent ± SD. *$P$ < 0.0002, 1-way ANOVA. (**E**) Scr HemSC/ECFC and N3KD HemSC/ECFC xenograft sections stained for αSMA. White arrowheads mark vessel surrounded by αSMA$^+$ mural cells. Yellow arrowheads mark vessel surrounded by mural cells that express low levels of αSMA. (**F**) αSMA$^+$ mural cell density determined as mean mural cell αSMA signal intensity normalized to IH endothelial GLUT1 signal intensity. Average mural cell αSMA expression determined as mean αSMA signal intensity–normalized DAPI$^+$αSMA$^+$ cell number ($n$ = 3 populations; $n$ = 2 implants each). Error bars represent ± SD. n.s., not significant. *$P$ < 0.0002, **$P$ < 0.000005, 1-way ANOVA. Scale bars: 50 μm. αSMA, α smooth muscle actin; ECFC, endothelial colony-forming cell; GLUT1, glucose transporter 1; HemSC, hemangioma stem cell; IH, infantile hemangioma, MC, mural cell; Scr, scrambled.

formation of smaller, more capillary-like vessels, leading to a reduction in the Dopplerable blood flow in the N3KD HemSC/ECFC implants. In the absence of the ECFCs, a significant decrease in vessel caliber and αSMA density was seen in N3KD HemSC implants relative to Scr HemSC implants (Supplemental Figure 9). A trend towards reduced mural αSMA expression was also observed. The data suggest that NOTCH3 has a pathological role in HemSC-to–mural cell differentiation in IH, leading to stabilization of the abnormal large-caliber vessels in involuting IH.

*Therapeutic NOTCH3 inhibition disrupted IH vessels in a mouse model of IH.* Next, we asked if therapeutic targeting of NOTCH3 could improve the IH vessel phenotype in the HemSC/ECFC mouse model. To block NOTCH3 signaling, we generated an N3 Decoy adenovirus that encodes the signal peptide and EGF-like repeats 1–24 of the NOTCH3 extracellular domain fused to human FC. In a coculture Notch signaling luciferase reporter assay, N3 Decoy blocked JAG1 activation of NOTCH signaling to a level similar to that of a γ-secretase inhibitor (GSI) (Supplemental Figure 10).

To model therapeutic targeting of an established IH lesion, HemSC/ECFC Matrigel implants were allowed to develop IH-like vessels for 3–7 days and the presence of Dopplerable vessels was confirmed (Supplemental Figure 11A). Mice were divided into 2 cohorts and intravenously injected with either

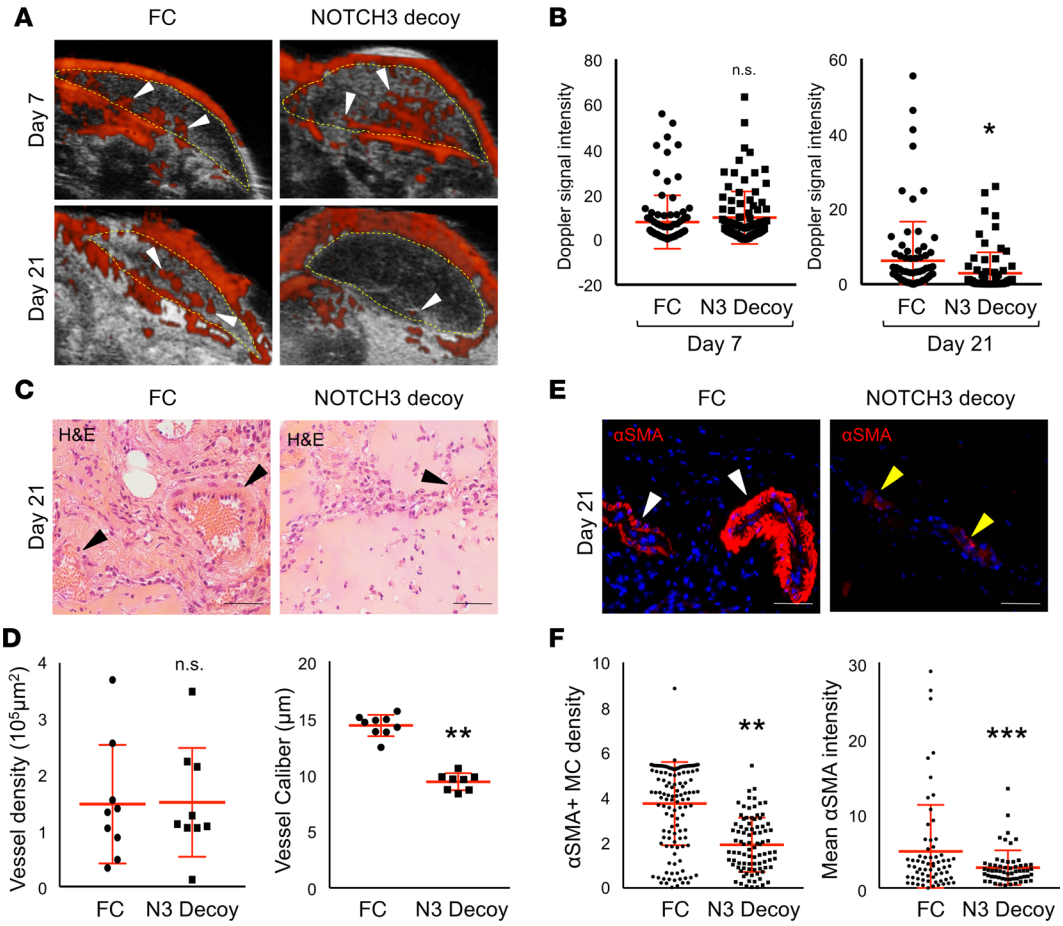


**Figure 6. A NOTCH3 inhibitor, NOTCH3 Decoy, blocks IH development and mural cell differentiation.** HemSCs and ECFCs in a 1:1 ratio were resuspended in Matrigel and implanted subcutaneously into immunocompromised mice. An adenovirus encoding NOTCH3 Decoy (N3 Decoy) or FC (control) was administered at either day 3 (H43, data not shown) or day 7 (H49) after implantation and IH development assessed until day 21 (schematic in Supplemental Figure 10A). (**A**) Detection of high blood flow by ultrasound Doppler of HemSC/ECFC xenografts prior to (day 7) and after (day 21) N3 Decoy and FC adenovirus injection. Xenograft area marked with yellow dotted line. White arrowheads mark Dopplerable blood flow (red). (**B**) Quantification of Doppler signal intensity normalized to implant area on day 7 and 21 ($n$ = 2 populations; $n$ = 4 implants each). *$P$ < 0.05, Student's $t$ test. (**C**) H&E staining of N3 Decoy– and FC-treated xenograft sections. Arrowheads mark red blood cell–containing vessels. (**D**) Quantification of vessel density and caliber ($n$ = 2 populations; $n$ = 4 implants each). **$P$ < 0.0005, Student's $t$ test. (**E**) N3 Decoy and FC HemSC/ECFC xenograft sections stained for αSMA. White arrowheads mark vessel surrounded by αSMA$^+$ mural cells. Yellow arrowheads mark vessel surrounded by mural cells that express low levels of αSMA. (**F**) αSMA$^+$ mural cell density determined as mean mural cell αSMA signal intensity normalized to IH endothelial GLUT1 signal intensity. Average mural cell αSMA expression determined as mean αSMA signal intensity–normalized DAPI$^+$αSMA$^+$ cell number ($n$ = 2 populations; $n$ = 4 implants each). n.s., not significant. **$P$ < 0.0005, ***$P$ < 0.01, Student's $t$ test. Scale bars: 50 μm. αSMA, α smooth muscle actin; ECFC, endothelial colony-forming cell; GLUT1, glucose transporter 1; HemSC, hemangioma stem cell; IH, infantile hemangioma, MC, mural cell; N3 Decoy; NOTCH3 Decoy; Scr, scrambled.

an adenovirus encoding N3 Decoy, or a control virus encoding FC. By this method, the adenoviruses preferentially infect the liver that then secretes either N3 Decoy or FC into circulation (Supplemental Figure 11B). Two weeks after adenoviral injection, Dopplerable blood flow was significantly decreased in mice expressing N3 Decoy as compared with the FC cohort (Figure 6, A and B). Similar to *NOTCH3* knockdown (Figure 5, C and D), N3 Decoy implants displayed a significant decrease in vessel caliber, but not vessel density (Figure 6, C and D). The reduced vessel caliber correlated with a decrease in αSMA$^+$ mural cell density and mural cell αSMA expression (Figure 6, E and F). To determine if the N3 Decoy affected the host vasculature, we analyzed the liver vasculature of mice with HemSC/ECFC implants. αSMA perivascular coverage did not differ between implanted mice expressing N3 Decoy or FC (Supplemental Figure 12). These findings demonstrate that N3 Decoy specifically targets the IH mural cells in the implants and that Notch3 signaling is necessary to maintain IH vessel integrity.

## Discussion

We demonstrate that mural cells have an essential role in IH progression. As perivascular mural cells are essential in stabilizing blood vessels in physiological angiogenesis, our study suggests that NOTCH3 functions in IH pathobiology to promote HemSC-to–mural cell differentiation that leads to abnormal IH vessel stabilization during the involuting phase.

In humans and mice, Notch3 is necessary for the proper differentiation and maturation of vascular pericytes and VSMCs in physiological angiogenesis (15). In humans, mutations in *NOTCH3* lead to CADASIL syndrome, a disorder associated with progressive arterial VSMC loss and microaneurysms beginning in the third decade of life (17, 18). Similar to CADASIL, mice nullizygous for *Notch3* are viable, but have progressive VSMC loss beginning around 2 months of age (19). Prior to VSMC death, VSMCs in *Notch3*-null mice have significantly reduced expression of smooth muscle myosin heavy chain (SMMHC) and smoothelin, reduced arterial vessel caliber, and impaired contractile function. Transgenic mice that express CADASIL *Notch3* alleles ubiquitously or in smooth muscle protein-22$^+$ (SM22$^+$) VSMCs also developed adult-onset VSMC death and decreased mechanotransduction (23–25). Studies using cultured cells have shown that the Notch ligand JAG1, expressed on ECs, activates NOTCH3 on the adjacent perivascular mural cell and induces expression of PDGFRβ and αSMA, as well as NOTCH3 in a positive feedback loop (16, 20). Consistent with in vitro studies, loss of endothelial *Jag1* is associated with reduced VSMC coverage in retinal angiogenesis (26, 27). Here, we demonstrate that NOTCH3 is necessary for mural cell differentiation in IH progression. We hypothesize that, similar to developmental angiogenesis, endothelial JAG1 serves as the NOTCH3 ligand in IH. In fact, knockdown of *JAG1* in ECFCs in the HemSC/ECFC cocultures inhibited HemSC differentiation into αSMA$^+$calponin$^+$ mural cells and IH blood vessel formation in the HemSC/ECFC xenograft model (10). Based on these observations, we propose that endothelial JAG1 signals to neighboring NOTCH3$^+$ HemSCs to promote mural cell differentiation during IH involution.

Our studies support roles for 2 distinct pathological cell populations in IH lesions: endothelial cells and perivascular mural cells that both contribute to IH development and progression. Proteins necessary for the differentiation and function of vascular mural cells, PDGFRβ, αSMA, NG2, and NOTCH3, are dynamically and improperly expressed as IHs progress from the proliferating to the involuting phase. During the early proliferative phase, PDGFRβ$^+$αSMA$^{lo}$NG2$^{lo}$NOTCH3$^+$ perivascular cells surround poorly organized lumenal CD31$^+$GLUT1$^+$NG2$^+$NOTCH3$^+$ HemECs. In the involuting phase, IH vessels consist of large-caliber vessels lined by CD31$^+$GLUT1$^+$PDGFRβ$^+$NG2$^+$ HemECs with spotty NOTCH3 expression surrounded by circumferentially oriented PDGFRβ$^{lo}$αSMA$^{hi}$NG2$^{lo}$NOTCH3$^+$ mural cells. The expression pattern of the mural cell proteins further suggests that both HemECs and mural cells in IH are improperly differentiated.

HemECs are distinct from ECs of the arteries, veins, and capillaries. They have a multilayered basement membrane, cuboidal morphology (1), express GLUT1 (4) that supports their increased metabolic activity, and have increased proliferation in response to VEGF (28). Paradoxically, HemECs are stimulated by the angiogenic inhibitor endostatin (28). We demonstrate that HemECs express both PDGFRβ and NG2, proteins not normally expressed in the mature endothelium. Although PDGFRβ and NG2 are considered mural cell markers in the vasculature (21, 22), both are expressed in progenitor cells. NG2 expression has been reported in bone marrow mesenchymal stem cells (29, 30), neuronal progenitor cells (31, 32), and lymphatic malformation progenitor cells (33). Similarly, PDGFRβ is expressed in circulating endothelial progenitors, as well as hemangioblasts (34, 35), suggesting that HemECs have failed to terminally differentiate from endothelial progenitor cells. A subset of the GLUT1$^+$ HemECs also expressed the mural cell marker NOTCH3, possibly representing a transitional cell type between the NOTCH3$^+$ HemSC and the NOTCH3$^-$ GLUT1$^+$ HemEC. Together, these data suggest that during the involution phase IH vessels consist of heterogeneous GLUT1$^+$ HemECs that misexpress progenitor cell/mural markers, NG2 and PDGFRβ, as well as NOTCH3. Recently, Huang et al. demonstrated IH vessels consisting of GLUT1$^+$ and GLUT1$^-$ HemECs, and that the GLUT1$^+$ HemECs displayed facultative stem cell properties (36), suggesting IH vessels are mosaics consisting of pathological GLUT1$^+$ ECs and normal GLUT1$^-$ ECs. Whether the abnormal expression of NG2 and PDGFRβ is restricted to only the GLUT1$^+$ HemECs remains to be elucidated.

Expression of PDGFRβ has been reported in proliferative and angiogenic ECs in both physiological and pathological conditions. Proliferating bovine aortic ECs expressed PDGFRβ in culture (37) and in microvasculature of the kidney (38). PDGFRβ expression has also been noted in the angiogenic ECs

in glioblastoma multiforme (39). Furthermore, blocking PDGFRβ in HUVECs blunted the angiogenic response induced by endothelial progenitor cell–conditioned media (40). Thus, misexpression of PDGFRβ in HemECs may contribute to the increased proliferation in HemECs and abnormal angiogenesis in IH.

Similar to HemECs, we propose that HemSC-derived mural cells improperly differentiate in IH and contribute to the blood vessel pathology. Consistent with the hypothesis that mural cells in IH are improperly differentiated, mural cells isolated from IHs have decreased contractility and when xenografted with ECFCs developed large-caliber IH-like vessels that were not observed in implants containing normal retinal mural cells (41). We demonstrate that mural cells in involuting IH specimens or induced from HemSCs in culture have reduced expression of PDGFRβ, a protein essential for mural cell organization and function (42–47). Loss of PDGFRβ activity during angiogenesis leads to endothelial hyperplasia and increased capillary caliber in the brain (45), and is associated with abnormal vascular patterning and permeability (47). Thus, even with NOTCH3 signaling, the loss of PDGFRβ in mural cells may contribute to IH vasculature pathology.

The mural cell coverage in involuting IHs may be secondary to the disrupted high-flow experience in IH vessels. Prolonged exposure to high flow increases VSMC coverage in arteries (48), and in arterial venous malformations the high flow experienced by the veins promotes VSMC association (48–50). Further studies are necessary to determine the role of flow in IH pathobiology.

We demonstrate that mural cells and NOTCH3 play critical roles in IH development and progression. Thus, NOTCH3 may be an effective therapeutic target, as inhibition of NOTCH3 could block vessel development and stabilization in IHs, leading to earlier resolution of the lesion. Unlike JAG1, which is widely expressed in multiple tissues and cell types and activates multiple Notch family members, NOTCH3 expression is highly enriched in perivascular cells (16, 20, 21). Thus, targeting NOTCH3 may have less adverse effects than JAG1 inhibition.

## Methods

*Tissue collection and cell isolation*. This study was approved by the Columbia Institutional Review Board (IRB-AAAA976). Resected IH clinical specimens were used for immunohistochemistry and cell isolation. All diagnoses of IHs were confirmed by clinical examination and histological confirmation of GLUT1 positivity in the specimen by our hospital clinical pathologist. Frozen tissues were fixed in 4% paraformaldehyde (PFA) overnight at 4°C, soaked in 30% sucrose in 1× PBS at 4°C, and frozen in OCT (Sakura Finetek). Paraffin-embedded tissues were fixed in 10% formalin overnight and dehydrated in ethanol and embedded in paraffin.

HemSC isolation and characterization were done as previously described (51, 52). In brief, proliferating regions of IH tissue were digested with collagenase, and HemSCs were isolated by $CD133^+$ magnetic bead selection (Miltenyi Biotech). HemSCs were cultured on fibronectin-coated (Corning) plates in Endothelial Cell Growth Media-2 (EGM-2, Lonza) supplemented with 20% FBS. ECFCs were provided by Joyce Bischoff (Harvard University, Boston, Massachusetts, USA) and isolated as previously described (53). ECFCs were cultured on fibronectin-coated plates in EGM-2 with 20% FBS.

*Constructs and cell line generation*. HemSCs lines were generated by lentivirus infection (54) using the pLKO vector encoding shN3 (N3KD), or scrambled sequence (Scr) (Sigma-Aldrich). N3KD and transgene expression were confirmed by qRT-PCR, immunohistochemistry, and Western analysis. Eight clones were tested and 1 of the 8 clones specifically knocked down *NOTCH3*, and this clone was used for subsequent experiments.

Adenoviruses were generated that encoded either N3 Decoy, which encodes EGF-like repeats 1–24 of NOTCH3 fused to human FC (Supplemental Figure 4), or FC alone as a control. Adenoviruses were produced and titrated as described (55).

*IHC*. Fixed frozen sections (5 μm) were stained with commercial antibodies (Supplemental Table 2) and detected with Alexa Fluor–conjugated secondary antibodies (Invitrogen) or with biotinylated-conjugated antibody and developed using a Vectastain ABC Kit and a DAB Peroxidase Substrate Kit (Vector Labs) as previously described (56). Colorimetric IHC slides were counterstained in Harris Modified Method Hematoxylin (Thermo Fisher Scientific), and coverslipped using Permount Mounting Medium (Thermo Fisher Scientific). Hematoxylin and eosin (H&E) staining was performed by the Herbert Irving Comprehensive Cancer Center pathology core at Columbia University. The total number of IH specimens assessed for each antigen is summarized in Supplemental Table 3.

For cell staining, HemSCs were seeded on fibronectin-coated 4-well Millicell EZ Slides (MilliporeSigma). After 24 hours, cells were fixed in 4% PFA on ice for 15 minutes, permeabilized with 0.1% Triton

X-100 in 1× PBS, and incubated with blocking solution (2% BSA, 3% donkey serum in 1× PBS) for 1 hour at room temperature before incubation overnight with primary antibody (Supplemental Table 2) at 4°C. The next day, slides were washed in 1× PBS, and incubated with fluorescently labeled secondary antibodies (Supplemental Table 2) for 45 minutes at room temperature. Slides were then washed in 1× PBS and coverslipped with Vectashield with DAPI mounting media (Vector). Images were captured with an Axiocam MRC system (Zeiss) and edited with Adobe Photoshop.

*Western analysis*. Cells were washed in cold 1× PBS and lysed with TENT buffer (PBS-T; 50 mM Tris pH 8.0, 2 mM EDTA, 150 mM NaCl, 1% Triton X-100) containing 1% HALT Protease Inhibitor (Thermo Fisher Scientific) and 1% Phosphatase Inhibitor (Thermo Fisher Scientific). Blots were incubated with blocking solution (4% BSA and 4% milk protein in 0.2% PBS-T) for 1 hour at room temperature, and primary antibody (Supplement Table 2) for 3 hours at room temperature. Blots were then washed in PBS-T, and incubated in HRP-conjugated secondary antibody for 45 minutes at room temperature. Blots were washed in PBS-T and detected with ECL Prime Western Blotting Detection Reagent (GE Life Sciences). Densitometry of bands of 300-dpi unmodified scans was determined using ImageJ version 6.0 (NIH) and results represented as the maximum pixel intensity minus the mean pixel density.

*FACS*. FACS analysis was performed for isolated HemSCs with antibodies against NG2, GLUT1, and PDGFRβ as described previously (34). Briefly, dissociated HemSCs were incubated with either protein-specific antibodies or matching IgG conjugated with either FITC or PE (Supplemental Table 2). FACS was performed using a FACSCalibur (BD Biosciences) and data analyzed with FlowJo Software.

*qRT-PCR*. qRT-PCR was performed as previously described (57). Briefly, RNA was isolated with the RNeasy Mini Kit (Qiagen), cDNA was synthesized using the SuperScript First-Strand Synthesis System (Invitrogen), and quantitative PCR performed with SYBR Green Master Mix (ABI) and gene-specific primers (Supplemental Table 4) using a CFX96 PCR Cycler (Bio-Rad). Gene-specific PCR products subcloned into pDrive (Stratagene) were serially diluted and used to generate a PCR standard curve. PCRs were normalized by *BACTIN* qPCRs.

*HemSC in vitro assay*. For mural cell differentiation, HemSCs were differentiated into mural cells using differentiation media (DMEM low glucose, Pen/Strep, FBS, TGF-β1) as described previously (34) and differentiation determined by staining for αSMA.

For coculture experiments, HemSCs were cocultured with ECFCs in growth media as described previously (11). HemSCs and ECFCs were cocultured in a 1:1 ratio on fibronectin-coated Millicell EZ Slides ($5.0 \times 10^3$ cells each) or 10-$cm^2$ plates ($5.0 \times 10^4$ cells). Cell mixtures were cultured for up to 9 days and HemSC differentiation was assessed by immunostaining or Western analysis for VSMC markers, αSMA and PDGFRβ.

*Mouse models of IH*. Mouse studies were performed with approval from Columbia University's Institutional Animal Care and Use Committee (AAAG5852, AAAO4900, and AAAQ8400). NCr nude females (strain *Foxn1nu*) 4–6 weeks old were used (Taconic). The xenograft IH mouse model was performed as previously described (51, 52). On day 0, $1.5 \times 10^6$ HemSCs suspended in 200 μl of Matrigel (Corning) were implanted subcutaneously into 7- to 9-week-old female NCr nude females (Taconic). On days 14 and 21, blood flow within the IH Matrigel implants was assessed by Doppler ultrasound (Vevo 2100, VisualSonics) as previously described (52). After 21 days, IH Matrigel implants were harvested, fixed in 10% formalin, and embedded in paraffin.

To assess the effects of ECFCs on HemSC differentiation in vivo, we used a modified xenograft IH mouse model. On day 0, $1.5 \times 10^6$ HemSCs and $1.5 \times 10^6$ ECFCs were suspended in 400 μl of Matrigel and injected subcutaneously into immunodeficient mice, and blood flow assessed by Doppler ultrasound on day 7 and 14. On day 14, IH coculture Matrigel implants were harvested and paraffin embedded.

For experiments with N3 Decoy, IH coculture implants were engrafted into immunodeficient mice as described above. Blood flow was assessed by Doppler ultrasound on day 3 or 7 to confirm IH development and blood flow prior to treatment. Mice were randomly divided into 2 cohorts and injected intravenously via the lateral tail vein with $5.0 \times 10^8$ focus-forming units (FFU) of adenovirus encoding either N3 Decoy or FC as a control. On day 14 or 21, blood flow was reassessed by Doppler ultrasound. Following Doppler ultrasound, mouse serum was collected by submandibular venous puncture. Mice were then sacrificed and IH Matrigel implants and livers were collected for histological and protein analysis. N3 Decoy and FC proteins were detected in liver samples by immunohistochemistry and Western analysis. FC was detected in serum by Western blot. N3 Decoy was detected in serum by immunoprecipitation with an antibody against FC and pulled down with protein A/G agarose beads (Santa Cruz Biotechnology) and subsequent Western blot for FC.

*Quantification methods*. For quantification of murine HemSC IH implants, 10 high-power fields (hpf) were imaged using the Axiocam MRC system (Zeiss). For quantification of murine coculture IH implants, an Olympus DP 80 camera mounted on an Olympus IX83 microscope and Olympus cellSens Dimension version 1.14 software was used to generate tiled images of entire sections of implants and quantified.

Vessels were identified as tubular structures with visible erythrocytes in H&E–stained sections (52). The number of vessels normalized to area and average vessel diameter was determined with ImageJ software. Areas of the matrigel were measured in microns$^2$ using ImageJ. VSMC coverage was determined for GLUT1$^+$ vessels by quantifying αSMA expression normalized to GLUT1 expression. Average αSMA expression levels were determined by measuring αSMA signal intensity and normalizing to the number of αSMA$^+$ nuclei (DAPI). Doppler ultrasound blood flow signal in implants was measured every 500 μm throughout the width of the implant-normalized by area. Blood flow signal was converted to a gray scale using ImageJ version 6.0 and pixel density quantified.

*Statistics*. To determine the significance between control and experimental groups, 2-sample independent-measures Student's *t* test was done using Excel, and scatter plots for Doppler blood flow and ANOVA was done with Prism version 6.0 software (GraphPad Software, Inc). A *P* value less than 0.05 was considered significant. The N3KD animal experiments were performed between 3 pairs of control/knockdown cell lines. Statistical significance between controls and knockdown for all 3 cell lines was determined using ANOVA, and Student's *t* test for intra–cell line comparisons.

*Study approval*. The collection of clinical specimens was approved by the Columbia University IRB (AAAA9976). The animal studies were approved by Columbia Institute for Animal Care and Use Committee (IACUC AAAG5852, AAAO4900, and AAAQ8400).

## Author contributions

AKE performed IHC for clinical and animal model tissues, in vitro differentiation assays and Western blots, animal experiments, Notch3 knockdown cell line generation, and contributed to the manuscript. KG performed IHC, in vitro differentiation assays, and Notch3 knockdown cell line generation. PG aided in the quantification of the animal models and performed FACS analyses. AAK aided in the quantification of the animal models and performed qRT-PCR experiments. NCOM performed qRT-PCR and IHC staining. KH performed Notch3 knockdown and qPCR experiments. QKT performed immunofluorescence of clinical specimens. MS performed IHC staining and qRT-PCR experiments. TK generated and validated the N3 Decoy protein. JKK provided advise and reagents and reviewed manuscript. CJS generated and validated the NOTCH3 Decoy protein, designed experiments, and revised the manuscript. JKW oversaw experiments and wrote the manuscript.

## Acknowledgments

The authors would like to thank Joyce Bischoff for providing ECFCs for our experiments.

Address correspondence to: June K. Wu, 161 Fort Washington Avenue, Suite 511, New York, New York 10032, USA. Phone: 212.342.3704; Email: jw92@cumc.columbia.edu.

1. Mulliken JB, Fishman SJ, Burrows PE. Vascular anomalies. *Curr Probl Surg*. 2000;37(8):517–584.
2. Léauté-Labrèze C, Harper JI, Hoeger PH. Infantile haemangioma. *Lancet*. 2017;390(10089):85–94.
3. Khan ZA, et al. Multipotential stem cells recapitulate human infantile hemangioma in immunodeficient mice. *J Clin Invest*. 2008;118(7):2592–2599.
4. North PE, Waner M, Mizeracki A, Mihm MC. GLUT1: a newly discovered immunohistochemical marker for juvenile hemangiomas. *Hum Pathol*. 2000;31(1):11–22.
5. Haggstrom AN, et al. Prospective study of infantile hemangiomas: clinical characteristics predicting complications and treatment. *Pediatrics*. 2006;118(3):882–887.
6. Drolet BA, Swanson EA, Frieden IJ, Hemangioma Investigator Group. Infantile hemangiomas: an emerging health issue linked to an increased rate of low birth weight infants. *J Pediatr*. 2008;153(5):712–715.
7. Shah SD, et al. Rebound growth of infantile hemangiomas after propranolol therapy. *Pediatrics*. 2016;137(4):1.
8. Smadja DM, Mulliken JB, Bischoff J. E-selectin mediates stem cell adhesion and formation of blood vessels in a murine model of infantile hemangioma. *Am J Pathol*. 2012;181(6):2239–2247.
9. Wu JK, et al. A switch in Notch gene expression parallels stem cell to endothelial transition in infantile hemangioma. *Angiogenesis*. 2010;13(1):15–23.
10. Boscolo E, et al. JAGGED1 signaling regulates hemangioma stem cell-to-pericyte/vascular smooth muscle cell differentiation.

*Arterioscler Thromb Vasc Biol*. 2011;31(10):2181–2192.
11. Guruharsha KG, Kankel MW, Artavanis-Tsakonas S. The Notch signalling system: recent insights into the complexity of a conserved pathway. *Nat Rev Genet*. 2012;13(9):654–666.
12. Rehman AO, Wang CY. Notch signaling in the regulation of tumor angiogenesis. *Trends Cell Biol*. 2006;16(6):293–300.
13. Bridges E, Oon CE, Harris A. Notch regulation of tumor angiogenesis. *Future Oncol*. 2011;7(4):569–588.
14. Adepoju O, et al. Expression of HES and HEY genes in infantile hemangiomas. *Vasc Cell*. 2011;3(1):19.
15. Liu H, Zhang W, Kennard S, Caldwell RB, Lilly B. Notch3 is critical for proper angiogenesis and mural cell investment. *Circ Res*. 2010;107(7):860–870.
16. Kofler NM, Cuervo H, Uh MK, Murtomäki A, Kitajewski J. Combined deficiency of Notch1 and Notch3 causes pericyte dysfunction, models CADASIL, and results in arteriovenous malformations. *Sci Rep*. 2015;5:16449.
17. Joutel A, et al. Notch3 mutations in CADASIL, a hereditary adult-onset condition causing stroke and dementia. *Nature*. 1996;383(6602):707–710.
18. Joutel A, et al. The ectodomain of the Notch3 receptor accumulates within the cerebrovasculature of CADASIL patients. *J Clin Invest*. 2000;105(5):597–605.
19. Domenga V, et al. Notch3 is required for arterial identity and maturation of vascular smooth muscle cells. *Genes Dev*. 2004;18(22):2730–2735.
20. Liu H, Kennard S, Lilly B. NOTCH3 expression is induced in mural cells through an autoregulatory loop that requires endothelial-expressed JAGGED1. *Circ Res*. 2009;104(4):466–475.
21. Armulik A, Genové G, Betsholtz C. Pericytes: developmental, physiological, and pathological perspectives, problems, and promises. *Dev Cell*. 2011;21(2):193–215.
22. Bergers G, Song S. The role of pericytes in blood-vessel formation and maintenance. *Neuro-oncology*. 2005;7(4):452–464.
23. Ruchoux MM, et al. Transgenic mice expressing mutant Notch3 develop vascular alterations characteristic of cerebral autosomal dominant arteriopathy with subcortical infarcts and leukoencephalopathy. *Am J Pathol*. 2003;162(1):329–342.
24. Dubroca C, et al. Impaired vascular mechanotransduction in a transgenic mouse model of CADASIL arteriopathy. *Stroke*. 2005;36(1):113–117.
25. Lacombe P, Oligo C, Domenga V, Tournier-Lasserve E, Joutel A. Impaired cerebral vasoreactivity in a transgenic mouse model of cerebral autosomal dominant arteriopathy with subcortical infarcts and leukoencephalopathy arteriopathy. *Stroke*. 2005;36(5):1053–1058.
26. High FA, Lu MM, Pear WS, Loomes KM, Kaestner KH, Epstein JA. Endothelial expression of the Notch ligand Jagged1 is required for vascular smooth muscle development. *Proc Natl Acad Sci USA*. 2008;105(6):1955–1959.
27. Benedito R, et al. The notch ligands Dll4 and Jagged1 have opposing effects on angiogenesis. *Cell*. 2009;137(6):1124–1135.
28. Boye E, Yu Y, Paranya G, Mulliken JB, Olsen BR, Bischoff J. Clonality and altered behavior of endothelial cells from hemangiomas. *J Clin Invest*. 2001;107(6):745–752.
29. Kozanoglu I, et al. Human bone marrow mesenchymal cells express NG2: possible increase in discriminative ability of flow cytometry during mesenchymal stromal cell identification. *Cytotherapy*. 2009;11(5):527–533.
30. Russell KC, et al. Cell-surface expression of neuron-glial antigen 2 (NG2) and melanoma cell adhesion molecule (CD146) in heterogeneous cultures of marrow-derived mesenchymal stem cells. *Tissue Eng Part A*. 2013;19(19–20):2253–2266.
31. Nishiyama A, Komitova M, Suzuki R, Zhu X. Polydendrocytes (NG2 cells): multifunctional cells with lineage plasticity. *Nat Rev Neurosci*. 2009;10(1):9–22.
32. Horner PJ, Thallmair M, Gage FH. Defining the NG2-expressing cell of the adult CNS. *J Neurocytol*. 2002;31(6–7):469–480.
33. Wu JK, et al. Aberrant lymphatic endothelial progenitors in lymphatic malformation development. *PLoS One*. 2015;10(2):e0117352.
34. Rolny C, et al. Platelet-derived growth factor receptor-beta promotes early endothelial cell differentiation. *Blood*. 2006;108(6):1877–1886.
35. Wang H, et al. Over-expression of PDGFR-β promotes PDGF-induced proliferation, migration, and angiogenesis of EPCs through PI3K/Akt signaling pathway. *PLoS One*. 2012;7(2):e30503.
36. Huang L, Nakayama H, Klagsbrun M, Mulliken JB, Bischoff J. Glucose transporter 1-positive endothelial cells in infantile hemangioma exhibit features of facultative stem cells. *Stem Cells*. 2015;33(1):133–145.
37. Battegay EJ, Rupp J, Iruela-Arispe L, Sage EH, Pech M. PDGF-BB modulates endothelial proliferation and angiogenesis in vitro via PDGF beta-receptors. *J Cell Biol*. 1994;125(4):917–928.
38. Lin SL, et al. Targeting endothelium-pericyte cross talk by inhibiting VEGF receptor signaling attenuates kidney microvascular rarefaction and fibrosis. *Am J Pathol*. 2011;178(2):911–923.
39. Plate KH, Breier G, Farrell CL, Risau W. Platelet-derived growth factor receptor-beta is induced during tumor development and upregulated during tumor progression in endothelial cells in human gliomas. *Lab Invest*. 1992;67(4):529–534.
40. Wyler von Ballmoos M, Yang Z, Völzmann J, Baumgartner I, Kalka C, Di Santo S. Endothelial progenitor cells induce a phenotype shift in differentiated endothelial cells towards PDGF/PDGFRβ axis-mediated angiogenesis. *PLoS One*. 2010;5(11):e14107.
41. Boscolo E, Mulliken JB, Bischoff J. Pericytes from infantile hemangioma display proangiogenic properties and dysregulated angiopoietin-1. *Arterioscler Thromb Vasc Biol*. 2013;33(3):501–509.
42. Soriano P. Abnormal kidney development and hematological disorders in PDGF beta-receptor mutant mice. *Genes Dev*. 1994;8(16):1888–1896.
43. Levéen P, Pekny M, Gebre-Medhin S, Swolin B, Larsson E, Betsholtz C. Mice deficient for PDGF B show renal, cardiovascular, and hematological abnormalities. *Genes Dev*. 1994;8(16):1875–1887.
44. Lindahl P, Johansson BR, Levéen P, Betsholtz C. Pericyte loss and microaneurysm formation in PDGF-B-deficient mice. *Science*. 1997;277(5323):242–245.
45. Hellström M, et al. Lack of pericytes leads to endothelial hyperplasia and abnormal vascular morphogenesis. *J Cell Biol*. 2001;153(3):543–553.
46. Gerhardt H, Betsholtz C. Endothelial-pericyte interactions in angiogenesis. *Cell Tissue Res*. 2003;314(1):15–23.

47. Jadeja S, et al. A CNS-specific hypomorphic Pdgfr-beta mutant model of diabetic retinopathy. *Invest Ophthalmol Vis Sci*. 2013;54(5):3569–3578.
48. Carlson TR, et al. Endothelial expression of constitutively active Notch4 elicits reversible arteriovenous malformations in adult mice. *Proc Natl Acad Sci USA*. 2005;102(28):9884–9889.
49. Uranishi R, Baev NI, Kim JH, Awad IA. Vascular smooth muscle cell differentiation in human cerebral vascular malformations. *Neurosurgery*. 2001;49(3):671–679.
50. Hoya K, Asai A, Sasaki T, Nagata K, Kimura K, Kirino T. Expression of myosin heavy chain isoforms by smooth muscle cells in cerebral arteriovenous malformations. *Acta Neuropathol*. 2003;105(5):455–461.
51. Wong A, Hardy KL, Kitajewski AM, Shawber CJ, Kitajewski JK, Wu JK. Propranolol accelerates adipogenesis in hemangioma stem cells and causes apoptosis of hemangioma endothelial cells. *Plast Reconstr Surg*. 2012;130(5):1012–1021.
52. Munabi NC, et al. Propranolol targets hemangioma stem cells via cAMP and mitogen-activated protein kinase regulation. *Stem Cells Transl Med*. 2016;5(1):45–55.
53. Khan ZA, et al. Endothelial progenitor cells from infantile hemangioma and umbilical cord blood display unique cellular responses to endostatin. *Blood*. 2006;108(3):915–921.
54. Tung JJ, Hobert O, Berryman M, Kitajewski J. Chloride intracellular channel 4 is involved in endothelial proliferation and morphogenesis in vitro. *Angiogenesis*. 2009;12(3):209–220.
55. Hardy S, Kitamura M, Harris-Stansil T, Dai Y, Phipps ML. Construction of adenovirus vectors through Cre-lox recombination. *J Virol*. 1997;71(3):1842–1849.
56. Vorontchikhina MA, Zimmermann RC, Shawber CJ, Tang H, Kitajewski J. Unique patterns of Notch1, Notch4 and Jagged1 expression in ovarian vessels during folliculogenesis and corpus luteum formation. *Gene Expr Patterns*. 2005;5(5):701–709.
57. Shawber CJ, Das I, Francisco E, Kitajewski J. Notch signaling in primary endothelial cells. *Ann N Y Acad Sci*. 2003;995:162–170.